

Convective Performance of Nanofluids in a Laminar Thermally Developing Tube Flow

Babajide Kolade

Kenneth E. Goodson

John K. Eaton

Department of Mechanical Engineering,
Stanford University,
Stanford, CA 94305-3030

While many of the published papers on nanofluids focus on measuring the increased thermal conductivity of the suspension under static conditions, the convective performance of these fluids has received relatively little attention. The present work measures the effective thermal conductivity of nanofluids under developing convective boundary layer conditions in tubes of diameter 5 mm. The experiments use a hydrodynamically fully developed laminar tube flow in the range $500 \leq Re \leq 1600$ with constant wall heat flux. The experiments were validated through measurements on pure de-ionized (DI) water, which results in a thermal conductivity value that agrees within 0.4% of handbook value. The increase in effective thermal conductivity for DI-water/ Al_2O_3 nanofluids is 6% for 2% volume concentration of Al_2O_3 , which is consistent with the previously reported conductivity values for this sample. For a suspension of multiwall carbon nanotubes in silicone oil, the thermal conductivity is increased by 10% over that of the base fluid for a concentration of 0.2% by volume. Scanning electron microscopy was utilized to examine the structure of the dry state of the nanotubes and elucidate the performance differences of carbon nanomaterials. [DOI: 10.1115/1.3013831]

Keywords: nanofluids, thermal conductivity, convective heat transfer, laminar flow, conjugate heat transfer, nanotube structure

1 Introduction

The term nanofluid is used to describe a suspension of nano-sized particles in a base fluid. Metals and crystalline solids have thermal conductivities that are orders of magnitude larger than those of liquids. Suspensions of particles of such materials are expected to have higher thermal conductivity than those of the base liquid. Suspensions with micron-/millimeter-sized particles exhibit enhanced thermal characteristics [1]. However, these slurries have drawbacks such as clogging and abrasion. The level of enhancement brought about by the inclusion of micron-/millimeter-sized particles is not as significant as suspensions with nanoparticles. It has been reported that the addition of small quantities of nanosized (10–300 nm) metals, metallic oxides, and carbon nanotubes significantly increases the thermal conductivity of the base fluid. For example, Eastman et al. [2] reported an increase of 40% in the thermal conductivity of ethylene glycol with the suspension of 0.3% by volume of 10 nm copper (Cu) particles. Such a marked increase has been attributed to the large surface area to volume ratio of nanoparticles [3] or the layering of fluid particles at the interface of included solid particles [4]. With these enhanced thermal characteristics and diminutive dimensions of the suspended particles, nanofluids are viable options as working fluids in such fields as microelectromechanical system (MEMS) technology, automotive cooling, high-speed computing, laser technology, and other energy intensive applications.

The majority of the published research works on nanofluids have focused on measuring the increased thermal conductivity of the suspension under stationary conditions. The conventional methods utilized for this purpose are the transient hot-wire (THW) method [2–7], the 3- ω method [8], and the parallel plate method [9].

There is considerable scatter in reported values of thermal con-

ductivity enhancement [10]. For example, Choi et al. [4] measured an increase of 160% in thermal conductivity of a synthetic oil, poly (α -olefin), with the addition of 1% by volume of multiwall carbon nanotubes (MWCNTs) using the THW method. Xie et al. [6], also using the THW method, measured an increase of only 19.6% with the addition of 1% by volume of MWCNT to decene (also an olefin), which has a base thermal conductivity of 0.14 W/m K. The THW technique and similar methods are susceptible to measurement errors; this may be due to the development of convection cells around the heater probe [11] or due to the temperature inhomogeneity in the sample caused by successive measurements [7].

Experimental work on the effect of nanoparticles in convective heat transfer has not been extensively or rigorously conducted. Xuan and Li [12] measured an increase of 39% in the Nusselt number in a turbulent fully developed flow in a tube, with constant heat flux, with the addition of 2% by volume of Cu nanoparticles (diameter <100 nm). Wen and Ding [13] studied the entrance region of a tube flow under laminar flow conditions, with constant heat flux. Their results showed an increase of over 40% in the convective heat transfer coefficient at an x/D location of 63 for the addition of 1.6% by volume of 27–56 nm Al_2O_3 particles to de-ionized water. However, there were significant errors in their baseline measurement of the thermal conductivity of water, casting doubt on the validity of the measurement. Similarly, Heris et al. [14] measured the effect of the addition of 20 nm aluminum oxide (Al_2O_3) particles to water in a constant wall temperature laminar tube flow. The tube inner diameter was 5 mm and the test section was 1 m long. They measured an increase of 10–30% in the convective heat transfer coefficient for a Péclet number ranging from 2500–6000 at 2% by volume concentration of Al_2O_3 . There is concern about the accuracy of their measurements of the sensible energy increase because they reported that the exiting flow temperature was measured using a thermocouple (TC) inserted directly into the flow line. For the Péclet number range they considered, the flow is not thermally fully developed and therefore a one-point measurement of the flow temperature within the test section is not representative of the mixed-mean temperature.

Contributed by the Heat Transfer Division of ASME for publication in the JOURNAL OF HEAT TRANSFER. Manuscript received February 11, 2008; final manuscript received October 7, 2008; published online March 19, 2009. Review conducted by Patrick E. Phelan.

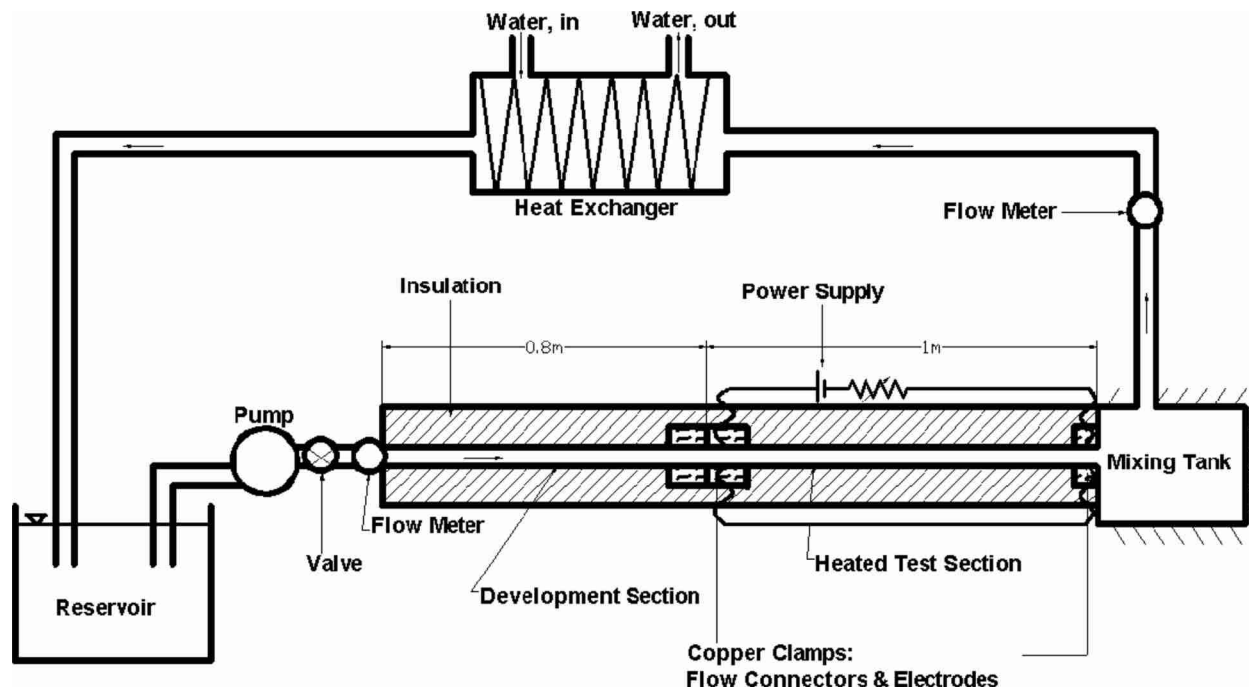


Fig. 1 Schematic of experimental setup

The main objective of the present work is to quantify the augmentation of the thermal conductivity of a liquid by the addition of nanoparticles in a convective environment. This experiment is conducted in a macroscale heat transfer apparatus; it is based on a laminar hydrodynamically fully developed flow in a tube, with constant heat flux. The heat transfer behavior in this simple flow is well understood, and the fluid conductivity can be extracted using only wall temperature measurements. Furthermore, the accuracy of the apparatus can be assessed by direct measurement of pure fluids for which the thermal conductivity is well known. Thus, the goal is to measure the effective thermal conductivity of a nanofluid in a convection application with a documented uncertainty of less than 0.04 W/m K .

2 Experimental Facility

A schematic of the experimental setup is shown in Fig. 1. The system is a closed recirculatory system. Fluid is pumped from the actively cooled reservoir, through a ball valve and a flow meter before entering a continuous stainless steel tube, comprising the development and test sections. The flow meter is a Micro Motion ELITE CMF025 Coriolis-type mass flow rate meter. This meter has the additional capability of measuring the density of the fluid. The flow exiting the test section passes into a mixing tank for the measurement of the mixed-mean temperature, through a heat exchanger, and then back to the reservoir.

The tube is thin walled and seamless, and it is made out of 316L stainless steel. It is 1.8 m long, with an inner diameter of 5.3 mm, and a wall thickness of 0.5 mm. The tube is partitioned into two sections: the development section, which is 0.8 m long, and the test section, which is 1 m long. The flow is allowed to develop hydrodynamically in the development section.

The inlet fluid temperature into the development section is measured by a sheathed, 0.8-mm-diameter, K-type thermocouple inserted into the flow at a location 2.5 mm from the entrance of the tube. Beaded, 36-gauge, K-type thermocouples are mounted on the external tube wall at three axial locations along the development section. In the test section, beaded K-type thermocouples made out of 0.13-mm-diameter (36-gauge) wires are mounted on the external wall of the tube at 19 axial locations. The thermocouples are attached using Omegabond® 101, a thermally conduc-

tive electrically insulating epoxy adhesive. Data from thermocouples used in this experiment were transferred to a zone box and recorded using an HP3497A multiplexer and a Fluke 8842A digital multimeter (DMM), at a sampling rate of 2.5 Hz. The mean and standard deviation are calculated for a sample size of 50 in the DI-water experiments and a sample size of 30 in the silicone oil experiments.

Constant heat flux is applied to the flow by means of Joule heating. Press-fit pairs of electrodes, made of electronic-grade copper, are mounted on the opposite ends of the test section at $x = 0.8 \text{ m}$ and $x = 1.8 \text{ m}$. These electrodes serve as junctions to the power supply, as well as ports for four-wire electrical measurements. An Agilent 6651 A dc power supply delivers current to the test section. This power supply is capable of delivering a maximum current of 50 A at 8 V and also measures the current flow. The voltage drop across the test section is measured using a Fluke 8842A digital multimeter and the current is measured by a Pace Scientific Model DC50A Hall-effect current sensor. The current measurement from the Hall-effect current sensor is compared with the measurement value provided by the power supply. The two values agree within 0.6% across the entire range of power input into the system. The resistance of the test section (0.085Ω), calculated from the voltage and current measurement acquired when the power supply is online, is corroborated by a four-point resistance measurement, acquired with the power supply off-line. These measurements agree within 0.5%. The maximum field strength applied axially for Joule heating in the experiments was 4 V/m. Because of the low value of the field strength and the low electrical conductivity of the nanofluid as compared with the tube, we assume that the Joule heating in the stainless steel tube will have negligible effect on the nanofluid heat transfer.

The entire tube is insulated in layers of polyethylene foam rubber insulation. The overall thermal resistance of the insulation is 12.3 K/W . The mixed-mean temperature of the flow exiting the test section is measured in an insulated mixing tank, using a sheathed K-type thermocouple. From the measurement of the mass flow rate and the inlet and exit flow bulk temperatures, the thermal energy conservation of the rig can be assessed. Since the

test section is well insulated, over 97% of the energy supplied by the power supply shows up as an increase in sensible energy of the test fluid.

3 Data Analysis and Rig Validation

The experimental measurements include mass flow rate, the applied electrical power, the mixed-mean temperature into and out of the tube, and the wall temperature at three points in the development section and 19 points in the heated section (test section). The goal of the analysis is to extract the fluid specific heat and the thermal conductivity. The accuracy of the measurement and data analysis procedures are verified by measuring the properties of pure fluids, as described in this section.

The specific heat is determined by a straightforward application of the conservation of energy as

$$C_p = \frac{P_E}{\dot{m}(T_{m,out} - T_{m,in})} \quad (1)$$

where P_E is the electrical power dissipated in the tube, and $T_{m,out}$ and $T_{m,in}$ are the mixed-mean temperature out and in of the tube, respectively. Note that there is no correction made for losses because the system is well insulated. To qualify the system, specific heat capacity was measured for pure de-ionized water at an average inlet temperature of 13°C and an average rise in bulk temperature of 4°C. All the measured values of specific heat were within 2.5% of the tabulated values. These qualification data show that the losses from the apparatus are small and that the specific heat can be measured with an uncertainty of 2.5% in the range of interest.

The experiment is modeled after a classic convective heat transfer problem, namely, the thermal entry region of laminar hydrodynamically fully developed round tube flow with constant heat flux. The analysis is complicated by the finite wall thickness of the tube, even though the tube wall thickness is small and the thermal conductivity of stainless steel is small relative to other metal tube materials. The product of the tube cross-sectional area and the stainless steel thermal conductivity was 1.6×10^{-4} W m/K. However, axial conduction through the tube wall was included in the data analysis procedure. The solution of the wall temperature rise in the stainless steel tube is derived from a conjugate heat transfer model of the experiment: Volumetric heat generation in the tube wall due to the Joule heating is balanced by convective heat transfer to the fluid, axial conduction, and losses through the insulation to the ambient.

The tube wall temperature profile was calculated using a finite volume scheme. The flow and the tube wall were discretized into unit cells. The energy balance for the fluid cell is as follows:

$$\dot{m}C_p(T_f^i - T_f^{i-1}) = (hA)^i(T_w^i - T_f^i) \quad (2)$$

In this equation, superscript i represents the i th cell in the discretization scheme; subscripts f and w denote the fluid and wall cells, respectively. An energy balance for a tube wall element is written as

$$q'''V_w + \frac{k_w A_w}{\Delta x}(T_w^{i+1} - T_w^i) = (hA)^i(T_w^i - T_f^i) + \frac{k_w A_w}{\Delta x}(T_w^i - T_w^{i-1}) + \frac{T_w^i - T_\infty}{R_{t,ins} + R_{t,amb}} \quad (3)$$

The terms representing the electrical heating generated in the wall and the axial conduction from the downstream wall element (on the left hand side of the equation) are balanced by the terms representing the transfer of thermal energy to the fluid, the axial conduction to the upstream wall cell, and the thermal energy loss through the insulation to the ambient. Variables q''' , V_w , k_w , A_w , and Δx represent the volumetric heat generation, the volume of the cell wall, the thermal conductivity of the tube wall, the cross-sectional area of the wall, and the discretization step length, res-

spectively. The variables $R_{t,ins}$ and $R_{t,amb}$ represent the thermal resistance of the insulation and the convective resistance from the insulation to ambient. These terms are defined as follows:

$$R_{t,ins} = \frac{\log[1 + t_{ins}/(r_o + t_w)]}{2 \cdot \pi \cdot \Delta x \cdot k_{ins}} \quad (4)$$

$$R_{t,amb} = [2 \cdot \pi \cdot (r_o + t_w + t_{ins}) \cdot \Delta x \cdot h_\infty]^{-1} \quad (5)$$

The variables r_o , t_w , t_{ins} , k_{ins} , and h_∞ represent the internal radius of the tube, the thickness of the tube wall, the thickness of the insulation, the thermal conductivity of the insulation, and the ambient convective heat transfer coefficient, respectively. A value of 5 W/m² K, estimated from empirical correlations [15], was used for the ambient convective heat transfer coefficient. Note that the modeling results are not sensitive to the assumed natural convective heat transfer coefficient within the range of 1–20 W/m² K. Apart from the heat transfer coefficient h , all the variables necessary for the conjugate analysis (solving Eqs. (2) and (3)) are known from the operating conditions or from geometrical parameters in the experiment.

In the case in which the temperature variation is small and the thermal properties of the fluid can be assumed constant, there is an infinite-series solution for the local Nusselt number [16].

$$Nu_x = \left[\frac{1}{Nu_\infty} - \frac{1}{2} \sum_{m=1}^{\infty} \frac{\exp(-\gamma_m^2 x^+)}{A_m \gamma_m^4} \right]^{-1} \quad (6)$$

The variable Nu_∞ is the asymptotic Nusselt number for a laminar constant heat flux problem and has a value of 4.364; x^+ is a non-dimensional axial location defined as $x/r_o/\text{RePr}$, where Re and Pr are the Reynolds number and Prandtl number of the flow, respectively. The eigenvalues and constants required for evaluating the expression may be found in Ref. [16]. For a known value of fluid thermal conductivity, Eqs. (2)–(6) can be combined to calculate a wall temperature distribution.

To facilitate the implementation of a numerical scheme, Eqs. (2) and (3) are rewritten, respectively, in the following form:

$$T_f^{i-1}(-X^i) + T_f^i(1 + X^i) + T_w^i(-1) = 0$$

$$T_w^{i-1}(Y^i) + T_w^i(1) + T_w^{i+1}(-1 - 2Y^i - Z^i) + T_w^{i+1}(Y^i) = -T_\infty(Z^i + Q^i)$$

where

$$X^i = \dot{m}C_p/(hA)^i, \quad Y^i = (k_w A_w/\Delta x)/(hA)^i$$

$$Z^i = [(R_{t,ins} + R_{t,amb}) \cdot (hA)^i]^{-1} \quad \text{and} \quad Q^i = q'''V_w/[(hA)^i \cdot T_\infty]$$

The tube is discretized into 100 cells. Forms of Eqs. (2) and (3) are written for each cell with appropriate boundary conditions. These equations are assembled into a matrix-vector form and the temperature profiles of the fluid and wall cells are solved for using MATLAB.

To validate the experimental setup, DI water with a known thermal conductivity of 0.6 W/m K is utilized as the working fluid in the experiment. Measured tube wall temperature values are compared with the temperature values calculated using the methodology described above. The comparisons for two operating conditions are shown in Figs. 2 and 3. Agreement between the measurement and theory is excellent, and within the estimated temperature uncertainty of 0.2°C.

4 Nanofluid Experiments

The augmentation in thermal conductivity is evaluated by comparing the tube wall temperature profile, at the same operating conditions, before and after the addition of nanoparticles to the base fluid. Two sets of base fluid/nanoparticles were investigated: a suspension of DI-water and 2% by volume of aluminum oxide (Al₂O₃) particles and a suspension of silicone oil (Dow Corning 200@ Fluid, 10 cS) and 0.2% by volume of MWCNTs. The characteristic viscosity of the silicone oil is 10 cS. The

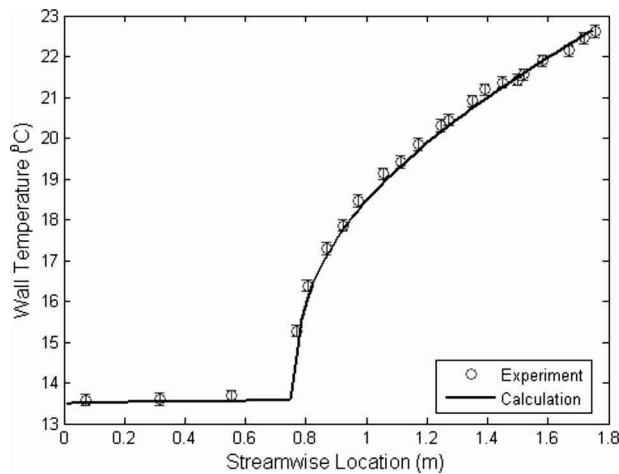


Fig. 2 Comparison of the measured and calculated temperature profiles in tube for nominal $Re=800$ and power output of 50 W

DI-water/ Al_2O_3 experiments were conducted for three conditions: three flow conditions (Reynolds numbers of 800, 1200, and 1600) at a power input of 50 W. The silicone oil/MWCNT experiments were conducted for four power settings (50 W, 100 W, 150 W, and 200 W) and two flow conditions (Reynolds number of 500 and 750). The values of kinematic viscosities of $1.0 \times 10^{-6} \text{ m}^2/\text{s}$ and $1.0 \times 10^{-5} \text{ m}^2/\text{s}$ were used to calculate nominal Reynolds number for the flow conditions in the DI-water/ Al_2O_3 and silicone oil/MWCNT experiments, respectively. Viscosity measurements were not performed for the nanofluids.

4.1 DI-Water/ Al_2O_3 Nanofluid Synthesis and Characterization. Spherical aluminum oxide particles, purchased from Alfa Aesar Corporation (Ward Hill, MA), were suspended in DI-water to produce the nanofluid. The Al_2O_3 particles were quoted to have a diameter of 40–50 nm. The particles had a purity of 99.5% and a specific gravity of 3.97 g/cm³. The as-produced particles were dispersed in water with the aid of a Hielscher UP400S titanium probe ultrasonic processor. Agglomerates created by interparticle bonding forces are disintegrated by jet streams emanating from ultrasonic cavitation created by the oscillation of the processor tip. The time necessary for the deagglomeration process was determined by fixing the intensive energy deposited into the suspen-

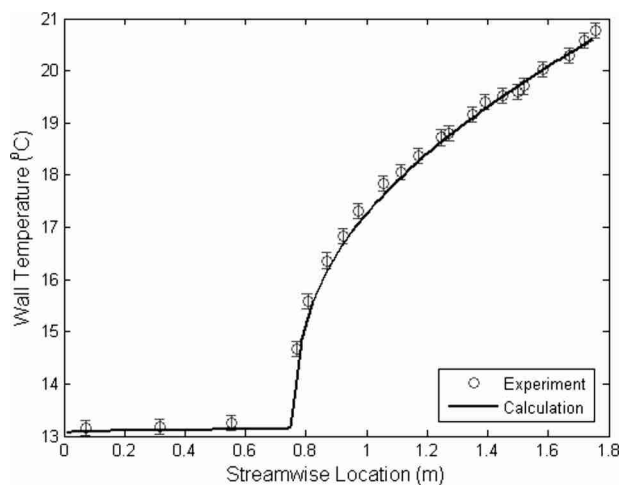


Fig. 3 Comparison of the measured and calculated temperature profiles in tube for nominal $Re=1200$ and power output of 50 W

sion. The intensive energy was fixed at $2.0 \times 10^9 \text{ J/m}^3$. Pohl and Schubert [17] reported that the deagglomeration process is independent of the particle loading concentration, up to 50% by volume particle loading.

According to the Derjaguin–Landau–Verwey–Overbeek (DLVO) theory, there is a balance between the attractive van der Waals forces and the electrostatic repulsion force, core repulsion force, and osmotic repulsion force [18]. This balance results in agglomerate sizes that differ from the particle size range quoted by the particle manufacturer. The particle size distribution in suspension was measured using a Brookhaven 90Plus Nanoparticle Size Analyzer, which employs the dynamic light scattering (DLS) technique.

In the DLS scheme, a laser beam incident on a volume in the colloidal sample is scattered in all directions. The colloidal sample is diluted so that single photon scattering is probable. The scattered beam is collected by a photomultiplier detector. In the case of the equipment used, the detector is static and is at a 90 degree angle from the incident beam. The photomultiplier collects the time autocorrelation of the light intensity, and the signal processing system determines the characteristic time delay for the scattered light to become random. Smaller particles diffuse faster within the scattering volume due to the Brownian motion, so the time autocorrelation is shorter for smaller particles. The time autocorrelation directly yields information about the diffusion coefficient of the particles. Given the diffusion coefficient and the viscosity of the base solvent, one may use the Stokes–Einstein equation to calculate the diameter of spherical particles.

The measured mean effective diameter of the particles in solution is 160 nm with a polydispersity of 0.14 (equivalent to a standard deviation of 57 nm), even though the manufacturer quoted a nominal particle size of 40–50 nm. Other researchers have also measured Al_2O_3 /DI-water nanofluid particle sizes larger than sizes quoted by the manufacturer. Ju et al. [7] measured an average particle size of 120 nm for Al_2O_3 particles that were quoted to be 30 nm. Lee et al. [19] studied the effect of different techniques on the dispersion of Al_2O_3 particles in water, using the same batch of particles as was used in the present work. The methods they employed included the modulation of the pH of the suspension, dispersion of the particles using both probe-type and bath-type ultrasonicators for varying periods of time, and the use of surfactants. They measured a mean effective diameter of the particles ranging from 140 nm to 230 nm, with a pH of 4 or lower resulting in the lower bound of mean effective diameter.

4.2 Silicone Oil/MWCNT Nanofluid Synthesis. The silicone oil used in the oil/MWCNT experiments has a nominal thermal conductivity of 0.15 W/m K, a kinematic viscosity of 10 cS, a density of 940 kg/m³, a specific heat capacity of 1600 J/kg K, and a Prandtl number of 100. The silicone oil selected for the experiment has thermal characteristics, at room temperature, similar to the thermal characteristics of engine oil at its operating conditions ($\sim 130^\circ\text{C}$). The results of the experiments may have direct applicability to engine cooling technologies. The MWCNT purchased from Sigma-Aldrich Inc. (St. Louis, MO) had quoted inside diameters of 5–10 nm, outside diameters of 10–30 nm, length of 0.5–500 μm , and a purity level of 95+%. The ultrasonic processor was used to deagglomerate the tubes in suspension. The intensive energy used in the deagglomeration process was $2.0 \times 10^8 \text{ J/m}^3$. The intensive energy used in this silicone oil/MWCNT synthesis is lower than in the DI-water/ Al_2O_3 because higher deagglomeration time, in the case of carbon nanotubes, seemed to have only marginal effects on the dispersion of the nanotubes in oil. The extent to which the nanotubes bundles were disentangled was not established. Dispersion of the nanoparticles was characterized using the DLS technique for the DI-water/ Al_2O_3 nanofluid experiments. In the silicone oil/MWCNT nanofluid experiments, dispersion was qualified by the settling time of the particles in suspension. The issue of the col-

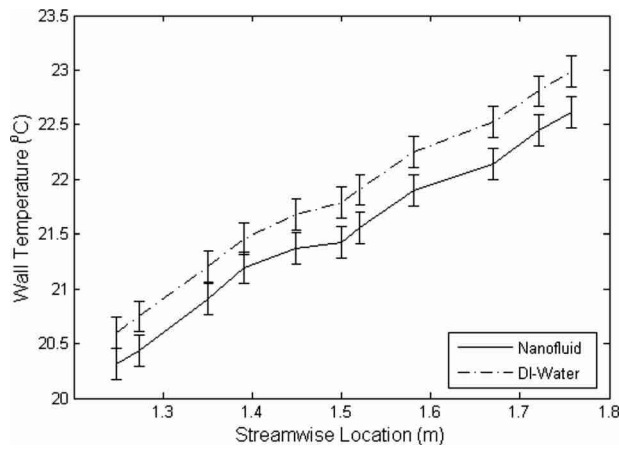


Fig. 4 Comparison of temperature rise in stainless steel tube for water and Al_2O_3 nanofluid at nominal $\text{Re} = 800$ and power input of 50 W

loidal stability is mitigated because the experimental setup is a recirculatory system. Experimental data taken a month apart, without draining and refilling the system, were identical.

5 Results and Discussion

Figure 4 shows a representative comparison of temperature rise in the wall of the stainless steel tube (test section) for the case of DI-water/ Al_2O_3 nanofluid for a Reynolds number of 800 and power input of 50 W. The wall temperature values for the experi-

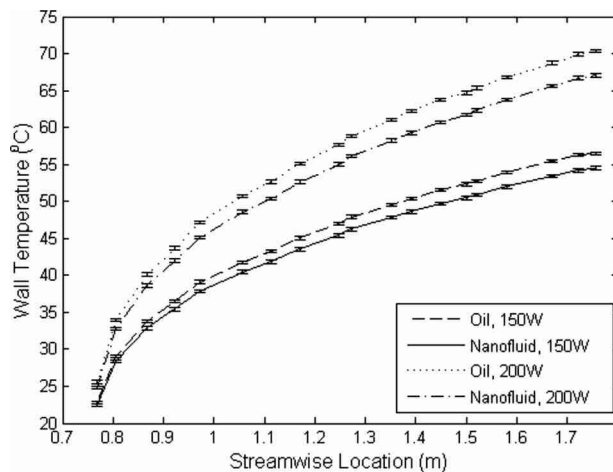


Fig. 5 Temperature rise in stainless steel tube for silicone oil and oil/MWCNT nanofluid at nominal $\text{Re} = 500$ and power input of 150 W and 200 W

ments using water were 0.4°C higher than that of experiments using the nanofluid. This difference in temperature is a reflection of the slight increase in the thermal conductivity of the working fluid.

Figure 5 shows comparisons between the wall temperature profiles in the test section for experiments run with silicone oil and silicone oil/MWCNT nanofluid. The Reynolds number of the flow is 500. The power inputs into the flow are 150 W and 200 W. There is a drop in the maximum wall temperature from the silicone oil cases to the nanofluid cases: 2°C for 150 W power input and 3.2°C for 200 W power input case. This temperature drop is indicative of the increase in thermal conductivity of the working fluid. The drop is more significant than that observed for the DI-water/ Al_2O_3 nanofluid. This suggests that the increase in thermal conductivity by suspending MWCNT in silicone oil is more significant than the increase in thermal conductivity by suspending Al_2O_3 in water, especially since only 0.2% by volume of MWCNT was suspended in the silicone oil.

5.1 Effective Thermal Conductivity. The heat input into the flow and wall temperatures are measured quantities in the experiment. For a constant heat flux experiment, the bulk temperature varies linearly with the axial position. Thus, the convective heat transfer coefficient may be directly calculated as $h = q'' / (T_w - T_f)$. For constant properties and hydrodynamically fully developed flow, there is an infinite-series solution for the Nusselt number [16]. The Nusselt number is a function of the nondimensional axial location x^+ , which is a function of the thermal conductivity: $x^+ = k / \rho \cdot C_p \cdot \bar{U} \cdot D$. The thermal conductivity may be calculated from the heat transfer coefficient and the Nusselt number: $k = h \cdot D / \text{Nu}$. Using this model for the Nusselt number, one can iteratively calculate the effective thermal conductivity of the fluid.

Single-sample uncertainty analysis is used in this work to quantify the uncertainties in the experimental results. This methodology was put forth by Kline and McClintock [20] and expanded on by Moffat [21]. Uncertainties in the wall temperature measurement, bulk temperature measurement, mass flow rate, and axial location of thermocouples were estimated. Uncertainties in the power input into the flow are accounted for by uncertainties in the change in the sensible energy of the liquid. These uncertainty values were propagated to the calculation of the effective thermal conductivity, using a 95% confidence interval.

The sources of uncertainties that were considered for the estimation of the uncertainty in the temperature measurements are thermocouple accuracy and resolution, digital multimeter accuracy and resolution, NIST K-type thermocouple conversion polynomial, and the standard deviation of the data set. The accuracy and resolution of the Coriolis meter and the standard deviation of the data set were considered as factors contributing to the uncertainty in the mass flow rate measurement. These sources of uncertainties and their associated numerical values are listed in Table 1.

Individual uncertainty estimates were calculated for each data point. The typical uncertainty in measuring thermal conductivity

Table 1 Uncertainty sources considered in uncertainty calculations

Device	Uncertainty source	Value
K-type thermocouples	NIST maximum voltage-to-temperature conversion error	$6.0(10)^{-2} \text{ }^\circ\text{C}$
K-type thermocouples	Accuracy of location of thermocouple (TC) beads	$1.6(10)^{-3} \text{ m}$
Digital multimeter (DMM)	DMM resolution for TC sampling	$1.0(10)^{-6} \text{ V}$
Digital multimeter	DMM accuracy in TC sampling	$2.0(10)^{-8} \text{ V}$
Current sensor	Fractional accuracy of measurement of power supply current	$6.0(10)^{-3}$
Digital multimeter	DMM resolution in measuring power supply voltage	$1.0(10)^{-4} \text{ V}$
Digital multimeter	DMM accuracy in measuring power supply voltage	$1.2(10)^{-3} \text{ V}$
Coriolis meter	Fractional accuracy of mass flow rate measurement	$3.0(10)^{-4}$
Coriolis meter	Resolution of Coriolis meter mass flow rate measurement	$2.1(10)^{-5} \text{ kg/s}$
Coriolis meter	Accuracy of density measurement	$2.0(10)^{-1} \text{ kg/m}^3$

Table 2 Uncertainty estimates for measured quantities

Quantity	Uncertainty
Wall temperature	$2.0(10)^{-1} \text{ }^\circ\text{C}$
Inlet flow temperature	$4.2(10)^{-2} \text{ }^\circ\text{C}$
Outlet flow temperature	$4.9(10)^{-2} \text{ }^\circ\text{C}$
Flow temperature rise	$6.5(10)^{-2} \text{ }^\circ\text{C}$
Mass flow rate	$5.7(10)^{-5} \text{ kg/s}$
Effective thermal conductivity (water-based experiments)	$3.0(10)^{-2} \text{ W/m K}$
Effective thermal conductivity (oil-based experiments)	$1.5(10)^{-2} \text{ W/m K}$

using this experimental methodology is 0.03 W/m K for water-based experiments and 0.015 W/m K for silicone oil-based experiments. The uncertainty estimates for the measured quantities are listed in Table 2.

Comparisons of the effective thermal conductivity calculated for DI-water-DI-water/ Al_2O_3 nanofluid and for silicone oil-oil/MWCNT nanofluid are shown in Figs. 6 and 7, respectively. Figure 6 shows an average thermal conductivity of water as 0.59 W/m K . This value compares well to the handbook value of 0.592 W/m K [16] at the average temperature of 15.3°C . The

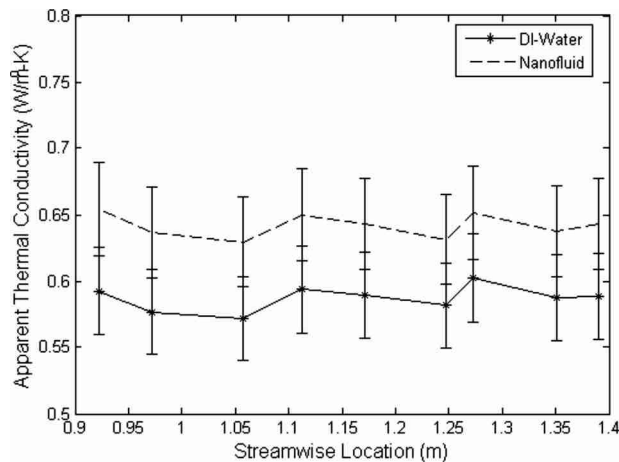


Fig. 6 Effective thermal conductivity for DI-water and DI-water/ Al_2O_3 nanofluid at nominal $\text{Re} = 800$ and power input of 50 W

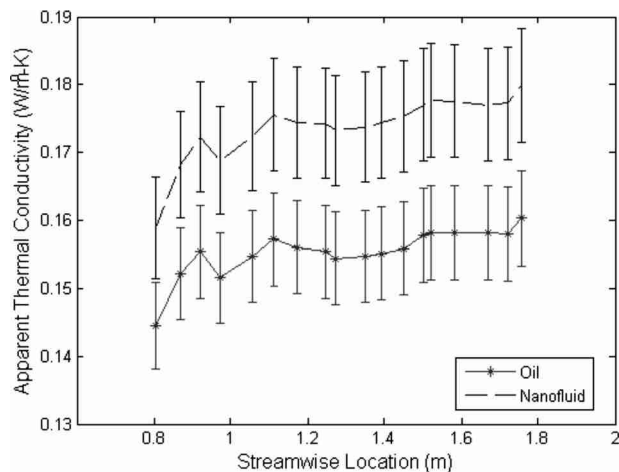


Fig. 7 Effective thermal conductivity of silicone oil and oil/MWCNT nanofluid at nominal $\text{Re} = 500$ and power input of 200 W

Table 3 Base fluid thermal conductivity of DI-water and augmentation of effective thermal conductivity by the addition of 2% by volume of Al_2O_3

Re	Power (W)	Base fluid thermal cond. ($\text{W/m}^2 \text{ K}$)	Nanofluid eff. thermal cond. ($\text{W/m}^2 \text{ K}$)
800	50	0.59	0.64
1200	50	0.61	0.64
1600	50	0.62	0.64

figure also shows an augmentation of about 8% in the thermal conductivity of DI-water by the addition of Al_2O_3 nanoparticles, at this operating condition. This increase in effective thermal conductivity is reflected by the decrease in measured wall temperatures for the DI-water/ Al_2O_3 nanofluid experiment, as shown in Fig. 4. Figure 7 shows an average thermal conductivity of silicone oil of 0.16 W/m K and an augmentation of around 12% by the addition of MWCNT, at that operating condition.

Similar experiments to those illustrated in Figs. 4–7 were run for a range of power settings and Reynolds numbers. The averaged values of measured thermal conductivities for DI-water and silicone oil are shown in Tables 3 and 4, respectively. Table 3 lists the measured values of thermal conductivity of water ranging from 0.59 W/m K to 0.62 W/m K . The handbook values of thermal conductivity are within the uncertainty range of the measured values. Table 4 lists the measured values of thermal conductivity of silicone oil ranging from 0.14 W/m K to 0.16 W/m K and the thermal conductivity of the silicone oil/MWCNT nanofluid ranging from 0.16 W/m K to 0.18 W/m K .

The intensive augmentation factor is defined as the percentage increase in thermal conductivity per percentage of volume of particles suspended. Averaged across the range of operating conditions, the addition of 2% by volume of Al_2O_3 nanoparticles to DI-water increased the thermal conductivity of water by 5.6%. Thus, the intensive augmentation factor for the DI-water/ Al_2O_3 nanofluid is 2.8. The addition of 0.2% by volume of MWCNT to silicone oil increased the thermal conductivity of the oil by 10.3%, averaged across the range of operating conditions; the thermal conductivity increased from a nominal value of 0.154 W/m K to a nominal value of 0.170 W/m K . The intensive augmentation factor of the oil/MWCNT nanofluid is 52.

Samples of the silicone oil and oil/MWCNT nanofluid that were used in this experiment were independently analyzed by Gharagozloo et al. [22]. They used a parallel plate method to measure the thermal conductivity of the oil and oil/MWCNT nanofluid under stationary conditions. Their experimental configuration was designed to minimize the development of convection cells. They measured a thermal conductivity of 0.151 W/m K for the silicone oil and a thermal conductivity of 0.175 W/m K for the oil/MWCNT nanofluid. A representative plot of their mea-

Table 4 Increase in effective thermal conductivity of silicone oil by the addition of 0.2% by volume MWCNT

Re	Power (W)	Base fluid thermal cond. ($\text{W/m}^2 \text{ K}$)	Nanofluid eff. thermal cond. ($\text{W/m}^2 \text{ K}$)
500	50	0.15	0.16
500	100	0.15	0.16
500	150	0.16	0.17
500	200	0.16	0.18
750	50	0.14	0.16
750	100	0.16	0.17
750	150	0.16	0.18
750	200	0.16	0.18

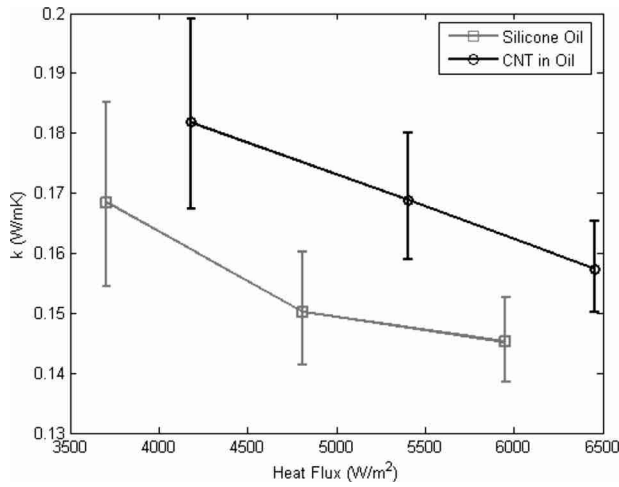


Fig. 8 Measurement of effective thermal conductivity of silicone oil and oil/MWCNT using parallel plate method [22]

surement is shown in Fig. 8. This measurement confirms the nominal value of the thermal conductivity of the pure silicone oil and indicates a 16% increase with the addition of 0.2% by volume of MWCNT. Therefore, both the convection and static experiments indicate an augmentation in thermal conductivity in excess of 10%.

5.2 Electron Microscopy Characterization. A different set of carbon nanomaterial, purchased from NanoCraft Inc. (Renton, WA). (Product: MWNT-A, No. 25921966870), was used to prepare nanofluid in the same procedure described above. Experiments with this batch of nanofluid did not indicate any increase in the thermal conductivity of the fluid. The wall temperature profiles in the test section in experiments utilizing this nanofluid were similar to wall temperature profiles in experiments utilizing only the base liquid. Figure 9 shows a comparison of the effective thermal conductivity of base fluid, the original nanofluid, and the new nanofluid, at a Reynolds number of 500 and a power input of 200 W. This plot demonstrates the repeatability of the methodology for calculating the augmentation in thermal conductivity and also shows the lack of the performance of the alternate nanomaterial.

The difference in the performance of the nanoparticles is attributed to the difference in the geometrical structure of the two sets

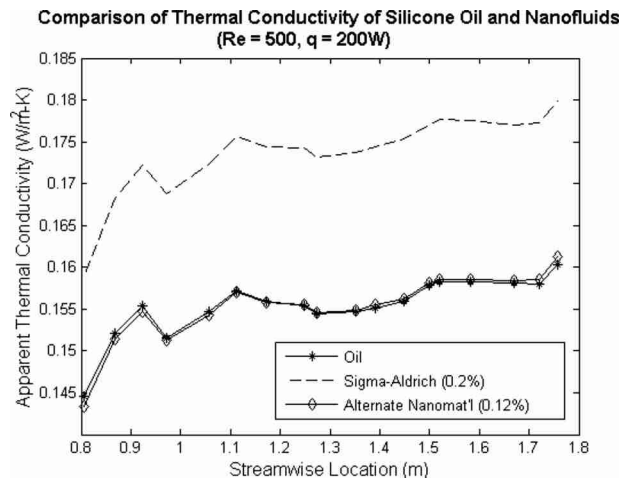


Fig. 9 Comparison of effective thermal conductivity of different nanofluids and silicone oil

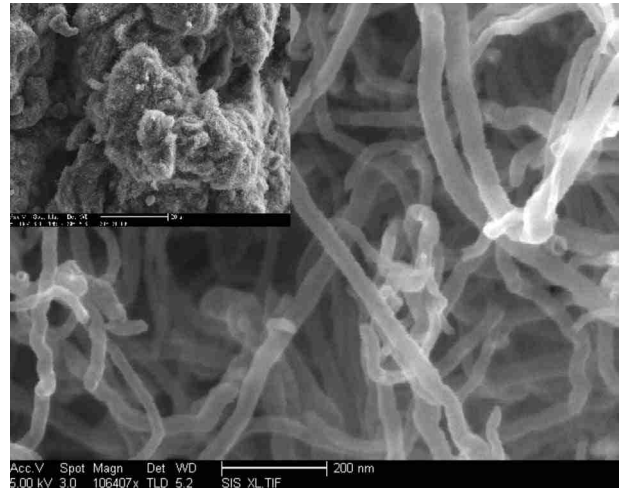


Fig. 10 SEM imaging of Sigma-Aldrich nanoparticles at a magnification of 100,000X. The inset is a 1500X magnification of the same sample.

of nanomaterials. Although they appear quite similar to the eye, the two materials show stark differences under magnification. Scanning electron microscopy (SEM) was utilized to examine the structure of the dry state of the nanotubes. The equipment used for SEM imaging is an FEI XL30 Sirion SEM, with FEG source and EDX detector. Figure 10 shows a sample of the Sigma-Aldrich nanotube under a 100,000X magnification; the inset in the picture is the same sample under a 1500X magnification. Figure 11 shows a similar size sample of the alternate nanomaterial under a 90,000X magnification; the inset in the picture is the alternate sample under 1500X magnification. The differences that start to become obvious in the 1500X magnification are glaring in the 90,000X / 100,000X magnification. Figure 10 shows an entangled bundle of nanotubes, whereas the material imaged in Fig. 11 has a semicrystalline nature. These differences in the material structure and aspect ratio are probably responsible for the thermal performance of the nanofluids.

6 Conclusions

The convective heat transfer performance of nanofluid in a hydrodynamically fully developed, thermally developing, laminar

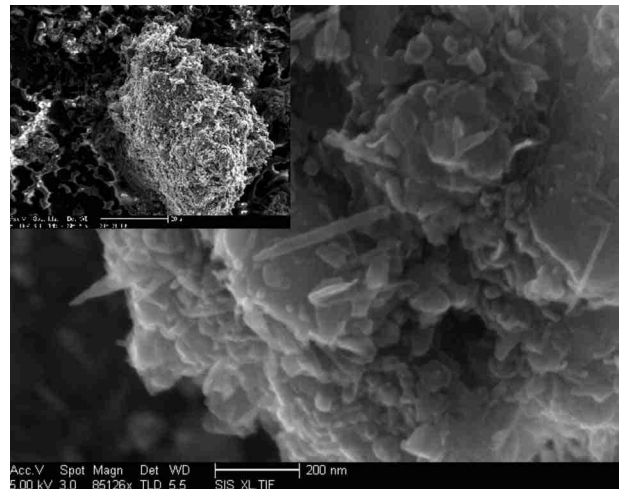


Fig. 11 SEM imaging of alternate carbon nanomaterial at a magnification of 90,000X. The inset is a 1500X magnification of the same sample.

tube flow, with constant heat flux, has been investigated. The experimental setup was first validated before the rig was used to measure the thermal conductivity of nanofluid. The validation methodology utilized standard heat transfer theory and conjugate heat transfer techniques to validate the experimental setup. DI-water/ Al_2O_3 nanofluid showed an intensive augmentation factor of about 3. This augmentation factor is more modest than what was earlier reported for some static measurements. Dynamic light scattering showed that the particle size in suspension was substantially larger than the size quoted by the supplier.

Oil/MWCNT nanofluid had an intensive augmentation factor of above 50. The thermal conductivity of the base liquid and the increase in thermal conductivity were corroborated by stationary parallel plate measurements. SEM imaging was used to visualize the dry state of the carbon nanotubes. The results of the carbon nanotube experiments suggest that the structure of the nanomaterial is an important factor in the augmentation of thermal conductivity of a liquid by the means of nanoparticles.

Acknowledgment

The authors would like to thank the Office of Naval Research Thermal Management Program, and Stanford University's School of Engineering Course Assistantship program for financial support. The authors would also like to acknowledge Anthony Burdi for his assistance in the development of the graphical interface for the data acquisition system and Andrew Lee for his assistance with SEM imaging.

Nomenclature

Δx	= discretization length, m
A_w	= cross-sectional area of tube wall, m^2
C_p	= specific heat capacity of fluid, J/kg K
h_∞	= ambient convective heat transfer, $\text{W/m}^2 \text{K}$
$(hA)^i$	= thermal conductance of i th fluid cell, W/K
k_{ins}	= thermal conductivity of insulation, W/m K
k_w	= thermal conductivity of tube wall, W/m K
\dot{m}	= mass flow rate of fluid, kg/s
Nu_x	= Nusselt number based on axial location
Pr	= Prandtl number of fluid
q'''	= volumetric heat generation, W/m^3
r_o	= radius of tube, m
$R_{t,\text{amb}}$	= thermal resistance of the ambient, K/W
$R_{t,\text{ins}}$	= thermal resistance of insulation, K/W
Re	= Reynolds number based on tube diameter
t_{ins}	= thickness of insulation, m
t_w	= thickness of tube wall, m
T_∞	= ambient temperature, K
T_f^0	= temperature of incoming fluid, K
T_f^i	= temperature of i th fluid cell, K
T_w^i	= temperature of i th wall cell, K
x	= dimensional axial location, m
x^+	= nondimensional axial location

$$V_w = \text{tube wall volume of a cell, m}^3$$

References

- [1] Ahuja, A. S., 1975, "Augmentation of Heat Transport in Laminar Flow of Polystyrene Suspensions," *J. Appl. Phys.*, **46**(8), pp. 3408–3425.
- [2] Eastman, J. A., Choi, S. U. S., Li, S., Yu, W., and Thompson, L. J., 2001, "Anomalously Increased Effective Thermal Conductivities of Ethylene Glycol-Based Nanofluids Containing Copper Particles," *Appl. Phys. Lett.*, **78**(6), pp. 718–720.
- [3] Lee, S., Choi, S. U.-S., Li, S., and Eastman, J. A., 1999, "Measuring Thermal Conductivity of Fluids Containing Oxide Nanoparticles," *ASME J. Heat Transfer*, **121**, pp. 280–289.
- [4] Choi, S. U. S., Zhang, Z. G., Yu, W., Lockwood, F. E., and Grulke, E. A., 2001, "Anomalous Thermal Conductivity Enhancement in Nanotube Suspensions," *Appl. Phys. Lett.*, **79**(14), pp. 2252–2254.
- [5] Eastman, J. A., Choi, U. S., Li, S., Thompson, L. J., and Lee, S., 1997, "Enhanced Thermal Conductivity Through the Development of Nanofluids," *Mater. Res. Soc. Symp. Proc.*, **457**, pp. 3–11.
- [6] Xie, H., Lee, H., Youn, W., and Choi, M., 2003, "Nanofluids Containing Multivalled Carbon Nanotubes and Their Enhanced Thermal Conductivities," *J. Appl. Phys.*, **94**(8), pp. 4967–4971.
- [7] Ju, Y. S., Kim, J., and Hung, M.-T., 2008, "Experimental Study of Heat Conduction in Aqueous Suspensions of Aluminum Oxide Nanoparticles," *ASME J. Heat Transfer*, **130**, pp. 092403.
- [8] Das, S. K., Putra, S., Thiesen, P., and Roetzel, W., 2003, "Temperature Dependence of Thermal Conductivity Enhancement for Nanofluids," *ASME J. Heat Transfer*, **125**, pp. 567–574.
- [9] Wang, X., Xu, X., and Choi, S. U. S., 1999, "Thermal Conductivity of Nanoparticle-Fluid Mixture," *J. Thermophys. Heat Transfer*, **13**(4), pp. 474–480.
- [10] Eastman, J. A., Phillpot, S. R., Choi, S. U. S., and Keblinski, P., 2004, "Thermal Transport in Nanofluids," *Annu. Rev. Mater. Res.*, **34**, pp. 219–246.
- [11] Ju, Y. S., and Kim, J., 2007, "Experimental Study of Heat Conduction in Aqueous Suspensions of Aluminum Oxide Nanoparticles," *Proceedings of IPACK2007*, ASME InterPACK '07, Vancouver, BC, Canada, Paper No. IPACK2007-32689.
- [12] Xuan, Y., and Li, Q., 2003, "Investigation on Convective Heat Transfer and Flow Features of Nanofluids," *ASME J. Heat Transfer*, **125**, pp. 151–155.
- [13] Wen, D., and Ding, Y., 2004, "Experimental Investigation Into Convective Heat Transfer of Nanofluids at the Entrance Region Under Laminar Flow Conditions," *Int. J. Heat Mass Transfer*, **47**, pp. 5181–5188.
- [14] Heris, S. Z., Esfahany, M. N., and Etemad, S. Gh., 2006, "Experimental Investigation of Convective Heat Transfer of Al_2O_3 /Water Nanofluid in Circular Tube," *Int. J. Heat Fluid Flow*, **28**, pp. 203–210.
- [15] Incropera, F. P., and DeWitt, D. P., 1996, *Fundamentals of Heat and Mass Transfer*, Wiley, New York, Chap. 9.
- [16] Kays, W. M., and Crawford, M. E., 1993, *Convective Heat and Mass Transfer*, McGraw-Hill, New York, Chap. 9.
- [17] Pohl, M., and Schubert, H., 2004, "Dispersion and Deagglomeration of Nanoparticles in Aqueous Solutions," *PARTEC*, pp. 1–4.
- [18] Stokes, R. J., and Evans, D. F., 1997, *Fundamentals of Interfacial Engineering*, Wiley-VCH, New York, Chap. 4.
- [19] Lee, J., Flynn, R. D., Goodson, K. E., and Eaton, J. K., 2007, "Convective Heat Transfer of Nanofluids (DI Water- Al_2O_3) in Microchannels," *Proceedings of HT2007*, ASME-JSME Thermal Engineering Summer Heat Transfer Conference, Vancouver, BC, Canada, Paper No. HT2007-32630.
- [20] Kline, S. J., and McClintock, F. A., 1953, "Describing Uncertainties in Single-Sample Experiments," *Mech. Eng.*, **75**, pp. 3–8.
- [21] Moffat, R. J., 1982, "Contributions to the Theory of Single-Sample Uncertainty Analysis," *ASME J. Fluids Eng.*, **104**, pp. 250–260.
- [22] Gharagozloo, P. E., Goodson, K. E., and Eaton, J. K., 2007, "Impact of Thermodiffusion on Temperature Fields in Stationary Nanofluids," *Proceedings of IPACK2007*, ASME InterPACK '07, Vancouver, BC, Canada, Paper No. IPACK2007-33293.